DEVELOPMENT OF SUPERSONIC NATURAL LAMINAR FLOW WING DESIGN SYSTEM USING CFD-BASED INVERSE METHOD

Hiroaki ISHIKAWA*, Keisuke OHIRA, Yoshifumi INOUE***, Kisa MATSUSHIMA**** and Kenji YOSHIDA*******
*** Sanko Soft Co.ltd, 2-14-2-1106, Takadanobaba, Shinjuku, Tokyo, 169-0075, Japan,**
**** Ryoyu Systems Co.,Ltd., 6-19 Oe-cho, Minato, Nagoya, 455-0024, Japan,**
***** Gakushuin University, 1-5-1 Mejiro, Toshima, Tokyo, 171-8588, Japan**
******University of Toyama, Gofuku 3190, Toyama, Toyama 930-8555, Japan**
******* Japan Aserospace Exploration Agency, 6-13-1, Osawa, Mitaka, Tokyo, 181-0015, Japan**

hiroaki@chofu.jaxa.jp

Keywords: supersonic, SST, NLF, CFD, inverse-method

Abstract

A supersonic natural laminar flow wing design system using computational fluid dynamics based inverse method is developed. A scaled supersonic experimental airplane called NEXST-1 (National EXperimental Supersonic Transport-1) has already been developed with a natural laminar flow wing design concept by using previous design system and verified the effect of its design concept by the flight test of Japan Aerospace Exploration Agency in 2005. The overall design system consists of the flow solver, a design module based on an inverse design problem and its interface module. Although the supersonic natural laminar flow wing could be designed by the previous design system, it was necessary to do much working load and human optimization process with some empirical knowledge. Those problems are improved with the present design system by using higher fidelity design method to eliminate the human optimization and applying automatic module to reduce the working load and the time span. The natural laminar flow wing design with the modified design system improves the transition locations compared with the result of the previous design system in spite of the drastically decreasing the working load and the time span.

1 Introduction

Supersonic transport (SST) is one of the promising future airliners with possibility to solve the growing airline demand and to liberate passengers from pain due to long flight time. One of the most important problems is its high fuel cost. Aerodynamic drag reduction solves the economical problem. Natural laminar flow (NLF) wing design technology is one of the most important solutions to reduce aerodynamic drag. Japan Aerospace Exploration Agency (JAXA) developed a scaled supersonic experimental airplane called NEXST-1 (National EXperimental Supersonic Transport-1) with NLF wing design concept (Fig 1.) and verified the effect of its concept by the flight test in 2005[1,2].

However, JAXA recognized some improvements of efficiency of its NLF wing design process, and also necessity of its extension to higher *Re* number condition of large supersonic transport. In this study, JAXA's NLF design system was modified to achieve the NLF wing design more accurately and efficiently. Then, this new design method was applied to the NEXST-1 airplane and compared with previous design method.

2 Design method

2.1 NLF wing design of NEXST-1

2.1.1 NEXST-1 airplane

The NEXST-1 airplane is a scaled supersonic experimental airplane with 11.5m of length and 4.72m of span as shown in Fig.1 which is the scale ratio of 11% of a future commercial SST planed by JAXA. It had no propulsion system because NEXST-1 was a gliding experimental airplane. Four design concepts, namely arrow wing planform, warped wing, area-ruled fuselage, and NLF wing were applied to the NEXST-1 to reduce aerodynamic drag at supersonic cruise condition (lift coefficient C_L=0.1 which was corresponding to angle of attack α=2.0deg and Mach number M=2.0). The arrow wing planform with an optimum slenderness ratio was selected from the supersonic linear theory[3] in compromising aerodynamics and structural constraints. Its aspect ratio was 2.2 and swept angle of the leading edge was 66 deg (in-board wing) and 61.2 deg (out-board wing) which were subsonic leading edge at M=2.0. To reduce lift-dependent drag, a warped wing was designed by using Carlson's method[4]. An optimum load distribution was able to be obtained by the optimum combination of wing camber and twist distributions. A supersonic area-ruled fuselage was also applied to reduce wave drag due to volume. The fuselage was designed so that the cross-sectional area distribution of overall shape of the aircraft is the same as that of the equivalent Sears-Haack body[5]. The NLF wing design concept is based on suppressing the Tollmien-Schlichting wave instability and the cross-flow instability. To suppress both instabilities, it is found an optimum pressure distribution using a practical transition prediction method with a linear stability analysis based on the e^N method[6,7].Then the NLF wing is designed from the above pressure distribution by using a CFD(Computational Fluid Dynamics)-based inverse design method[8] on the expected flight test condition (altitude H=15km, M=2.0, the MAC(=2.754m) based Re=22.212x10^6[3], C_L=0.1, α=2.0deg). Then, the wing configuration which has similar pressure distributions to the target ones was designed by JAXA's CFD-based inverse design method. The advantage of this inverse design method is to be able to design an NLF wing geometry without boundary layer transition analysis which would be needed much time to obtain the boundary layer transition characteristic.

The effects of its design concepts have been already verified by the flight test in 2005[1,2] by JAXA. The laminar flow region is observed in the design point by the some boundary layer transition measurement systems.

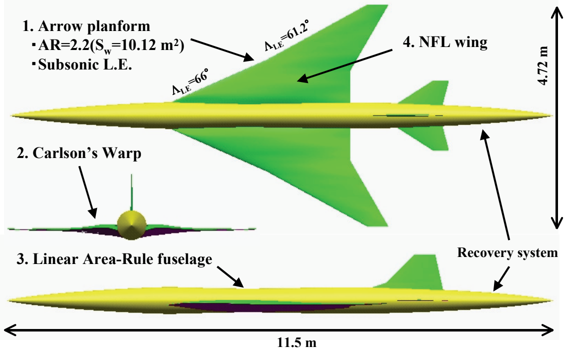

Fig 1. NEXST-1 configuration

2.1.2 Inverse design process

The supersonic NLF wing design system using CFD based inverse design method is performed along the described design process in Fig.2. First of all, baseline configuration is determined with the other design concepts, namely arrow wing planform, warped wing, area-ruled fuselage. Then the baseline configuration is smoothed if it is necessary. Next, the computational grid on the smoothed surface and in the space is generated for CFD analysis. Then CFD analysis is conducted in order to obtain the surface C_P distribution of the wing surface. The C_P distribution by CFD is compared with the target C_P distribution. Where, the target C_P distributions on the upper wing surface of the baseline configuration are determined by using linear stability analysis. If the C_P distribution by CFD is corresponding enough to the target C_P distribution, the design process is finished. If the C_P distribution by CFD is not satisfied the convergent criteria, NLF wing is designed by using the inverse design method. In this paper, the determination of the target pressure distribution, the CFD analysis method, the inverse design method and the evaluation of the design are shown in detail below sections.

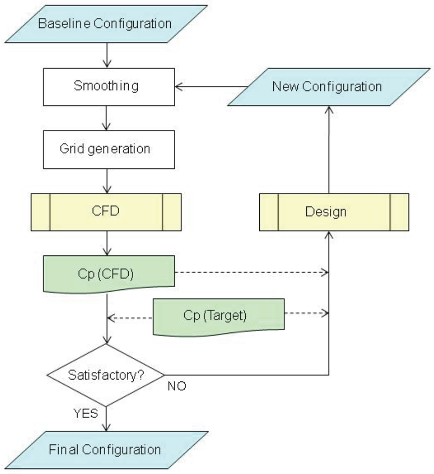

Fig 2. Design process of the NLF wing

2.1.3 Target Pressure distributions

The target C_P distributions are obtained by two design concepts. On the upper wing surface target C_P distributions are determined by NLF wing design concept[6,7,8]. The differential pressure distributions between the upper surface and lower surface on each wing section are obtained from the Carlson's warp design[4]. Then, the lower target C_P distributions are defined by adding these differential C_P distributions to the upper distributions.

The upper wing surface target C_P distributions are obtained by using boundary layer analysis and linear stability analysis. The boundary layer profile included density, velocity, temperature and pressure is obtained by boundary layer analysis from arbitrary pressure distribution on the wing surface. Then linear stability analysis is conducted using LSTAB[7] code which is JAXA's in-house code based on e^N method. In this target C_P distribution determination process, N value is assumed 14. Figure 3 shows the target C_P distributions at the in-board cross section(y/s=0.3) and the out-board cross section(y/s=0.7). These target pressure distributions have a sharply increased pressure gradient at the narrow region of the front part of the wing, and have gradual pressure gradients at other chord locations. It is found that the discrepancies are observed between the target C_P and the baseline C_P which is corresponding to the initial shape of the NLF wing design phase. The baseline C_P distributions should move closer to the target ones.

The boundary layer transition on-set positions are also estimated by the transition analysis based on e^N method(N=14). Figure 4 shows the boundary layer transition analysis results from obtained target C_P distribution and the baseline configuration at the altitude H=15 km (design point) and the H=18 km (the flight test condition). "Baseline" shows predicted boundary layer transition position using its C_P distributions from the CFD analysis. Baseline transits almost around the leading edge (x/c=0.03-0.4). On the other hand, the boundary layer transition position by the target C_P distributions is located backward region. Therefore, it is indicated that the target C_P distributions has potentially NLF wing characteristic. This tendency is shown from both conditions that are different Re number conditions (altitude,H=15 and 18km).

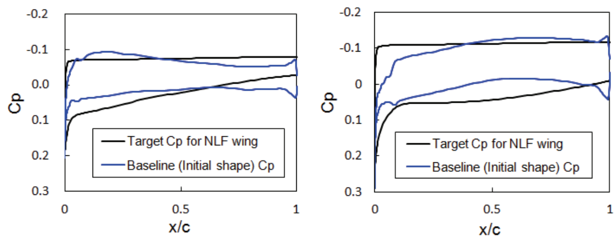

(a) y/s=0.3(in-board) (b) y/s=0.7(out-board)

Fig 3. The target C_P distributions

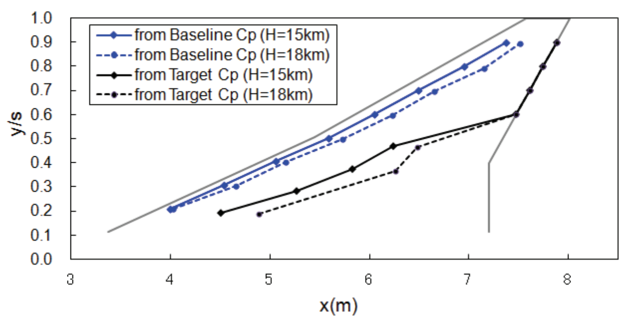

Fig 4. Estimated boundary layer transition on-set(N=14). H=15km is design point, H=18km is flight test condition

2.1.4 CFD analysis method

The multi-block structured grid CFD solver called UPACS(Unified Platform for Aerospace Computation Simulation)"[9] is used in this NLF wing design process. The multi-block structured grid code (UPACS), which is developed by JAXA, is based on a cell-centered finite volume method, in which the convection terms of the governing equations are discretized using Roe's flux difference splitting scheme with the MUSCL 2nd order extrapolation and vanAlbada limiter. MFGS (Matrix Free Gauss-Seidel) implicit method is used for time integration. In this design process, viscosity effect is considered because the wing camber is slightly changed by the displacement thickness comes from the viscosity effect. The governing equation is RANS (Reynolds averaged Navier-Stokes) equation with fully turbulent flow to prevent laminar separation on the wing surface. However, UPACS has some turbulence model options. In this study, The Baldwin-Lomax model[10] is used to simulate turbulent flow which is the lowest working load for the computation in the turbulence models of UPACS.

2.1.5 Inverse design method

The inverse design[8] system determines the wing section geometry, whose coordinate is (x,y,z), and equation to express a wing surface is $z=f(x,y)$. The x coordinate is chord-wise and the y coordinate is span-wise direction as shown in Fig.5. The z coordinate is in the wing thickness direction. The inverse problem of the design part should handle the Δ-value, which is difference between two states of a flow field. The goal of the formulation is to obtain the mathematical function to relate ΔC_P to geometrical correction of wing surface Δf. Performing Green's theorem and calculus on the flow equation of the small perturbation approximation on a flow field about a thin wing, it is obtained following equations, Eqs.(1)-(6). These inverse design equations are divided into wing thickness part and wing camber part. In these equations $\beta=\sqrt{M_\infty^2-1}$.

Wing thickness part:

$$\Delta w_s(x,y)=-\Delta u_s(x,y) -\frac{1}{\pi}\int_{\tau_+}\int\frac{(x-\xi)\Delta w_s(\xi,\eta)}{\left[(x-\xi)^2-(y-\eta)^2\right]^{3/2}}d\eta d\xi \tag{1}$$

where

$$\Delta u_s(x,y)=-\frac{1}{2\beta^2}(\Delta Cp_+ +\Delta Cp_-) \tag{2}$$

$$\Delta w_s(x,y)=-\frac{1}{\beta^3}\frac{\partial}{\partial x}(\Delta f_+ -\Delta f_-) \tag{3}$$

Wing camber part:

$$\Delta w_a(x,y)=-\Delta u_a(x,y) -\frac{1}{\pi}\int_{\tau_+}\int\frac{(x-\xi)\Delta u_a(\xi,\eta)}{(y-\eta)^2\sqrt{(x-\xi)^2-(y-\eta)^2}}d\eta d\xi \tag{4}$$

where

$$\Delta u_a(x,y)=-\frac{1}{2\beta^2}(\Delta Cp_+ -\Delta Cp_-) \tag{5}$$

$$\Delta w_a(x,y)=-\frac{1}{\beta^3}\frac{\partial}{\partial x}(\Delta f_+ +\Delta f_-) \tag{6}$$

Eqs.(1) and (4) are the basic equations to determine the geometrical correction. The subscript + indicates that the variable is on the upper surface of the wing while the subscript – indicates the lower surface. The area for integration, denoted by τ_+, is the upper wing surface limited by the forwarded Mach cone from a point $P(x,y)$ and leading edge line. P is located at the center of every panel on the wing where the discretized equations are evaluated. The integral area τ_+ the triangular planform and P are also shown in Fig.5. In Eqs.(1) and (4), ξ and η are integral variables which respectively correspond to x and y in the integration area(τ_+). Namely, it is considered the three-dimensional effect by not only the chord–wise variable(x,ξ) but also the span-wise variables(y,η). Eq.(1) is a Volterra integral equation of the second kind for Δw_s. Δw_s is associated with the chord-wise thickness change at (x,y) on a wing. Eq.(4) is the integral expression for Δw_a, which is associated with the chord-wise curvature change of the wing section camber, at (x,y).

The unknown geometrical correction function, Δf, which is the z coordinate change of the wing surface, is calculated using $\Delta w_s(x,y)$ and $\Delta w_a(x,y)$;

$$\Delta f_{\pm}(x, y/\beta) = \frac{1}{\beta^3}\int_{L.E.}^{x}\left[\Delta w_s(\xi, y) \pm \Delta w_a(\xi, y)\right] d\xi \quad (7)$$

Consequently the z coordinate value on the wing surface of the next generation ($f_{n+1}(x,y)$) is expressed as below.

$$f_{\pm,n+1}(x,y) = f_{\pm,n}(x,y) + \lambda_{n+1} \cdot \Delta f_{\pm,n+1}(x,y) \quad (8)$$

where n means previous design generation and n+1 is the next design generation. The λ_n is a relaxation coefficient for the geometrical correction function. When the λ_n=1.0, the next generation geometry fully takes in the geometrical correction Δf. However, sometimes the full geometrical correction induces unexpected divergent pressure distributions. In this case, the under 1.0 relaxation coefficient (λ_n<1.0) is applied in order to avoid the divergent tendency.

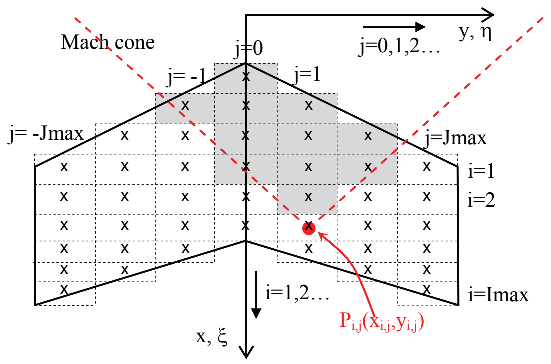

Fig 5. Coordinates and panels for formulation of the inverse problem of wing design

2.1.6 Evaluation of the design shape

As for criteria to judge the design completed, two kind of evaluation method are introduced.

Fist one, which is applied to the inverse design cycle, is quantitative criterion of the difference from the target to the current pressure distributions. The role of the inverse design method is to obtain a wing shape which realizes the prescribed target pressure distribution. The design results are evaluated by how the resulting pressure distribution agrees with the target one. To evaluate this quantitatively agreement, an objective function is defined as

$$I = \frac{\int_{y/s_{\min}}^{y/s_{\max}} \oint_{up\&low} \left|C_{p,design} - C_{p,taget}\right| d(x/c)\, d(y/s)}{\int_{y/s_{\min}}^{y/s_{\max}} \oint_{up\&low} d(x/c)\, d(y/s)} \quad (9)$$

where $y/s_{\min}$ and $y/s_{\max}$ indicate design region. In the NEXST-1 airplane design process, the span width region is defined from y/s=0.12 to y/s=0.9. In the actual inverse design process, more detail parts of the pressure difference should be monitored to obtain a higher performance natural laminar wing. The Eqs.(9) could be transformed to obtain the breakdown objective function easily. When these objective functions drop below a sufficient level or saturate during last few cycles, the inverse design cycle is finished.

The other criterion is to estimate how wide NLF area is realized on a wing surface. After the inverse design cycle is finished, the stability analysis[7] based on e^N method is performed to predict the transition location on the upper wing surface. If the laminar boundary layer area is over 50%, the NLF design of the NEXST-1 airplane could complete.

2.2 Previous design method

At first, the previous design method[1,8] is explained in this subsection. Table 1 shows a summary of NLF design method comparing the previous design method with present modified method. A new configuration should be smoothened to generate the CFD grid, because an intermediate configuration after one iteration of design phase has generally some numerical oscillations and discontinuous which could induce unexpected pressure distributions with oscillations and discontinuous. The smoothing treatment was manually conducted by commercial software “CATIA”. Software operating skill and special technical know-how were required for the smoothing process. For example, the operator searched and eliminated the element caused oscillations and discontinuous, then the implemented smoothing tool was run. Because the manually smoothing process takes much working load, only 14 cross sections could be treated with 1.5days. And if the computational grid for CFD analysis is also manually generated, it takes 1day. Furthermore, at the optimization phase of the previous design method, so-called "human" optimization is normally applied in order to obtain more accurate design from some candidate configurations by a sensitivity study. This "human" optimization generally needs researcher's knowledge with high quality, a lot of database and also design time. Thus it is strongly required to develop more accurate and efficient automatic design method without "human" optimization.

Table 1. NLF wing design method

	Previous design	Modified design
Smoothing of Wing geometry	Manually smoothing by CAITA from 14 cross sections (1.5day)	Automatically smoothing based on Conformal mapping by Auto-COMPAW (in-house code) from 90 cross sections (few minuets)
Grid Generation	Manually generation by GRIDGEN (1day)	Automatically generation by Auto-COMPAW (in-house code) and GRIDGEN with script (few minuets)
CFD	RANS with coarse mesh by NWT (old JAXA's super computer) (3days)	RANS with fine mesh by JSS (present JAXA's super computer) (8hours)
Target Cp	Upper surface : NLF wing by Linear Stability analysis on 9 section to span width direction Lower surface : Carlson warp Stagnation : from empirical data (fixed)	Upper surface : NLF wing by Linear Stability analysis on 90 section to span width direction Lower surface : Carlson warp Stagnation : modified by each CFD result
Design	Inversed design method based on Panel method with Ackeret's 1st-order approximation for Cp on 50(chord)x82(span) panel and human optimization	Inversed design method based on Panel method with Busemann's 2nd-order approximation for Cp on 150(chord)x100(span) panel
time required/1 cycle	1 week	1 day
total cycles	7 cycle with some candidates	10 cycles

2.3 Modification of the design method

2.3.1 Modification overview

In order to solve the previous design method problems as mentioned above, the NLF wing design method was modified. The right column of Table 1 shows its representative features of the modified design.

In the smoothing of the wing geometry part, an automatically smoothing system based on conformal mapping transformation is developed and applied. It is explained in detail next subsection. Using the automatically smoothing system, the working term is decreased from 1.5days to few minutes.

After the wing geometry smoothened, the computational grid is generated by using an automatically grid generation system based on "GRIDGEN" with script. The grid generation system becomes simple, because the surface grid of the wing is already generated by the wing smoothing process. The grid generation term is decreased from 1day to few minutes.

The computational grid density becomes higher than before. The previous grid has 100(chord) x 100(span) points on the upper wing surface and the present grid has 160(chord) x 160(span) points to obtain a more accurate flow field data as shown in Fig.6. The computational time is decreased by the improvement of the supercomputer performance.

The target C_P distribution is as almost same as the previous one. The stagnation position and the stagnation C_P value are only changed. In the previous design, these are determined by empirical data and fixed during the NLF design. On the other hand, in the modified design, these are updated by using the prior CFD analysis results, because the stagnation value of each cross section are changed during the design cycle by some reasons such as forward shock wave and the variable wing cross section. Thus the target C_P distribution is changed from the leading edge to x/c=0.03 on the lower surface.

The present inverse design method was also modified by adding Buseman's 2nd-order approximation for C_P distribution. And the panel for the inverse design method is increased from 50(chord) x 82(span) to 150(chord) x 100(span) in order to obtain the more accurate geometrical correction.

In this modified design method, the new configuration was designed by only inverse design method without any "human" optimization to reduce the workload and time. As a result of such effect of the "non-human" optimization, the number of panels and CFD grid points were increased at the modified design method. And required time for one design cycle was drastically decreased from 1 week to 1 day approximately.

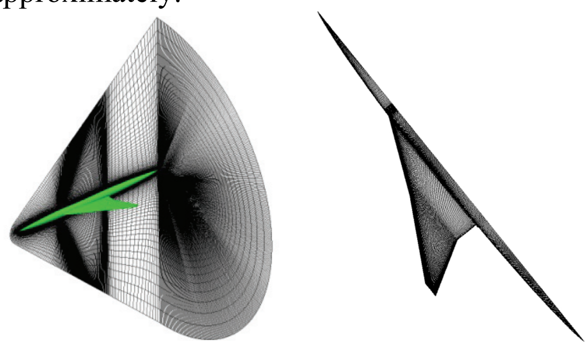

(a) boundary surface (b) wall surface

Fig 6. Present computational grid

2.3.2 Wing shape smoothing

The next generation design shape is obtained by adding the geometrical correction function(Δf) on the discrete panel of previous geometry in the inverse design process. The new design shape generally have some oscillations and discontinuous which should be removed in order to perform the high quality NLF design. In particular, it is desirable to define the geometry of wing cross section by using a continuous function to smooth the first derivative and second derivative of the geometry. In this study, the idea of a conformal mapping used in the fluid analysis of two-dimensional potential flow is applied into the smoothing of the two-dimensional wing cross section. Figure 7 shows that the smoothing process with conformal mapping. First of all, the arbitrary wing cross sections with twist angle are transformed to physical plane with un-twist and scaled into the 1.0 chord length. In this subsection, the physical plane,z is assumed below.

$$z = x + iy \tag{10}$$

And the mapping plane,ζ is assumed by using an angle variables θ as below.

$$\zeta = \xi + i\eta = \cos\theta + i(\sin\theta) \tag{11}$$

The geometry in the physical plane can be defined by the conformal mapping function expanded into a complex form of Fourier series by using Imai's[11,12] expansion method as below.

$$z = f(\zeta) = \sum_{n_c=-1}^{N_c} \left(P_{n_c} + iQ_{n_c}\right)\zeta^{n_c} \tag{12}$$

In the Eqs.(10-12), the real part shows the chord width direction value,x and the imaginary part shows the height direction value,y. In other words, The wing cross section can be expressed by the conformal mapping function (continuous function) with only the angle variable,θ and the continuity of the geometry can be maintained. Then the new design geometry on the new CFD grid points is generated by the inverse transformation after the definition of the angle variable,θ which is corresponding to the x/c of the previous geometry CFD grids. Although the greater order n_c value could provide the better reconstructed geometry, a possibility that the unexpected oscillation would occur becomes high. After the performing a parametric study, it is found that the appropriate smoothing order,n_c is 15th order.

Then the wing geometry at each cross section should be smoothened along the span width direction because of the three-dimensional configuration. If the geometrical value such as z

is smoothened, the continuity of the wing cross section might be lost. In this smoothing process, the coefficients of the conformal mapping function(P_n,Q_n) are smoothened by using polynomial equation from least squares approximation. At the same time, the wing cross sections are retransformed to the twist wing using the twist angle, τ(deg) by the least squares approximation polynomial, because the flat wing is used in the wing cross section smoothing as mentioned above. It is also conducted a parametric study about the order of the polynomial. And it is found that the appropriate smoothing order,n_s is 12th order.

Finally, the variables for the definition of the planform such as the leading edge position and the chord length are directly used from the base-line geometry (the initial geometry) because of keeping the original planform including kink position discontinuity.

The using cross sections into the shape smoothing process are increased from 14 sections to 90 sections which are almost all sections of the result from the inverse design. At the final analysis, the term of the smoothing process is drastically decreased from 1.5days to few minutes by the effect of present automation system, even though the using cross section increases.

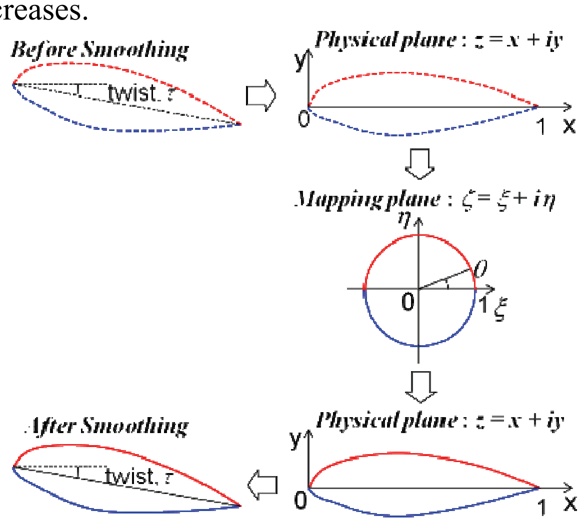

Fig 7. Smoothing image by conformal mapping

3 Results and Discussion

3.1 Modification design (1st trial)

The NEXST-1 airplane was re-designed by using present modified design method as mentioned above. Figure 8 shows the C_P distribution of the baseline configuration called "0th design". In the design cycles, the airplane configuration is simplified by elimination of the tail wing. At the first trial using the modified NLF design method called "Mod.1", it is conducted by using above design method. The relaxation coefficient λ of the inverse design method (Eqs.8) is fixed to 1.0 which means that the geometrical correction is directly used to obtain the next generation design shape. The NLF design cycle is performed from 0th to 10th. Figure 9 shows that history of the objective function from Eqs.9. The objective function is rapidly decreased until 3rd design and it looks like saturation to 5th design. After that, it is increased from 6th design. In order to clarify where the divergence tendency comes from, the local objective function at the different y/s position is investigated. Figure 10 shows results of the local objective function at y/s=0.3 (in-board) and y/s=0.7 (out-board). At the in-board cross section (y/s=0.3), it is observed that the objective function is decreased to 10th design. On the other hand, at the out-board cross section (y/s=0.7), the local objective function is increased after 6th design. That might be the reason of the global objective function divergence after 6th design. Figure 11 shows the breakdown results which are divided into the upper and lower surface, and furthermore into quarters of the chord direction such as x/c=0-0.25, 0.25-0.5, 0.5-0.75 and 0.75-1.0. Thus, the global objective function is divided into 8 regions like the illustration in the Fig.11. Although the objective function from x/c=0.25-1.0 is decreased step by step, the objective function from x/c=0.0-0.25 is increased after 6th design. This fact indicates that the divergence tendency after 6th design in the global objective function caused from near the leading edge. And it is found the leading edge in x/c=0-0.25 occupies over half of the total. The NLF wing is important around the leading edge of rapid gradient pressure distribution. To be converged the differential between the target pressure distribution and the designed shape's one around the leading edge is a big question to achieve the NLF wing.

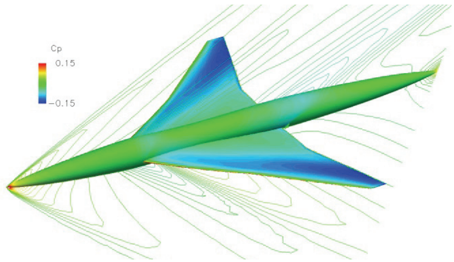

Fig 8. C_P distribution of the 0th design shape

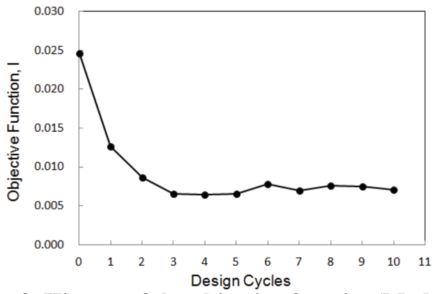

Fig 9. History of the objective function(Mod.1)

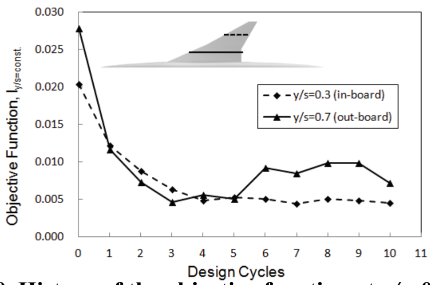

Fig 10. History of the objective function at *y/s*=0.3,0.7

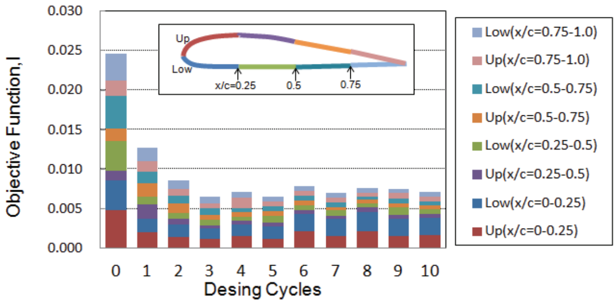

Fig 11. Breakdown history of the objective function (Mod.1)

3.2 Modification design (2nd design)

To solve the above problem of the "Mod.1" design, it is investigated several approaches such as changing some parameters. Then, it is found the relaxation coefficient λ in the geometrical correction Δf (Eqs.8) is dominant for the out-board divergence tendency and over estimated in case of λ=1.0. It is performed with changing the relaxation coefficient from λ=1.0 (Mod.1) to λ=0.5 started from the 3rd design configuration of the "Mod.1". In this paper, the second one is called "Mod.2". Figure 12 shows that the global objective function compared with the "Mod.1" design and the "Mod.2" one. At the 6th design cycle, the objective function is decreased. The smoothing order for span direction at the 5th design cycle is forced to reduce because the grid generation does not work for some reason. It is suggested that the grid generation system should be modified for more efficient NLF wing design. Anyway, the objective function after the 6th design cycle is decreased step by step without any divergences. It is suggest that the half relaxation coefficient λ=0.5 is effective for the convergence of the NLF wing design. This fact is observed from the local objective function in each cross section. Figure 13 shows that the representative local objective function at *y/s*=0.3 and 0.7. Each local objective function is increased after 6th design cycle and shown saturation around 9th design cycle. Especially, the out-board section (*y/s*=0.7) is drastically improved by the effect of the relaxation coefficient. This effect is also observed by the 8 parts breakdown of the global objective function as shown in Fig.14. The objective function is decreased not only afterward region (*x/c*=0.25-1.0) but also the leading edge region (*x/c*=0-0.25). Especially, the reduction near the leading of the "Mod.2" design is much better than afterward region compared with the reduction of the "Mod.1" design (Fig.11).

And then, see the wing section geometry and the C_P distribution on the *y/s*=0.3 and 0.7. Figure 15 and 16 show the wing section geometry at the *y/s*=0.3 and 0.7 respectively. And Fig.17,18 and 19 show the C_P distribution on the wall surface, the *y/s*=0.3 and 0.7 respectively. The results of the "Mod.2" are shown the 10th designed shape. The wing section airfoils of the "Mod.2" looks like "Mod.1" and little bit different from "Mod.1". As expected from the history of the objective function at the local cross section (Fig.13), although no significant C_P difference at the *y/s*=0.3, the C_P distribution at the *y/s*=0.7 is significantly improved and is closer to the target C_P distribution. The oscillations shown in the "Mod.1" at the *y/s*=0.7 are disappeared in the "Mod.2". It is found that the half of the relaxation coefficient (λ=0.5) is effective for better NLF design wing.

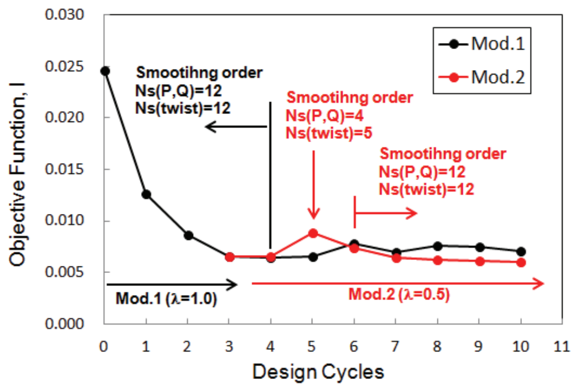

Fig 12. History of the objective function ("Mod.1" vs. "Mod.2")

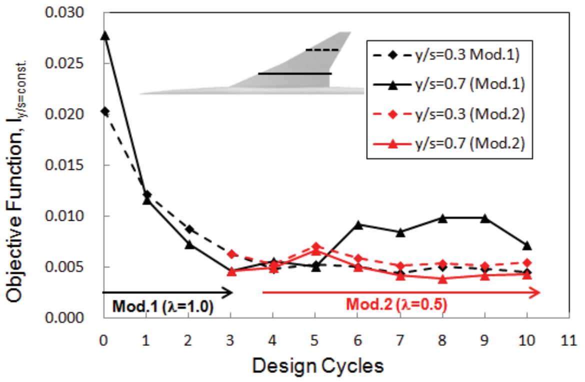

Fig 13. History of the objective function at y/s=0.3,0.7 ("Mod.1" vs. "Mod.2")

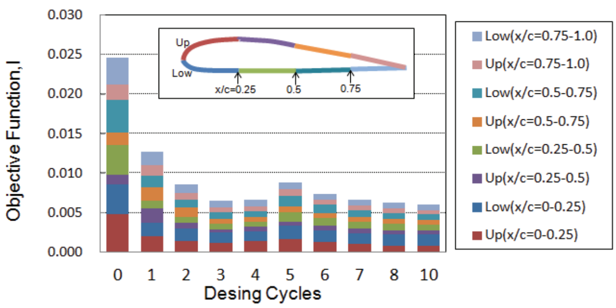

Fig 14. Breakdown history of the objective function (Mod.2)

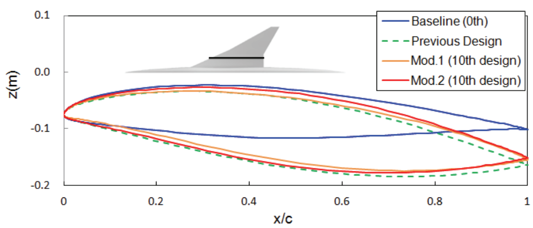

Fig 15. Wing cross section airfoil (y/s=0.3)(Mod.2)

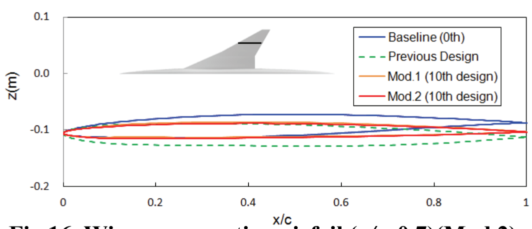

Fig 16. Wing cross section airfoil (y/s=0.7)(Mod.2)

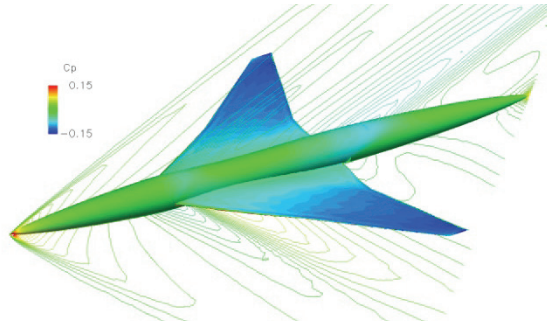

Fig 17. C_P distribution of the 10th design shape (Mod.2)

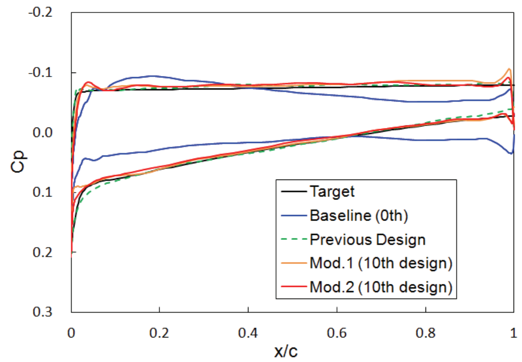

Fig 18. C_P distributions (y/s=0.3)(Mod.2)

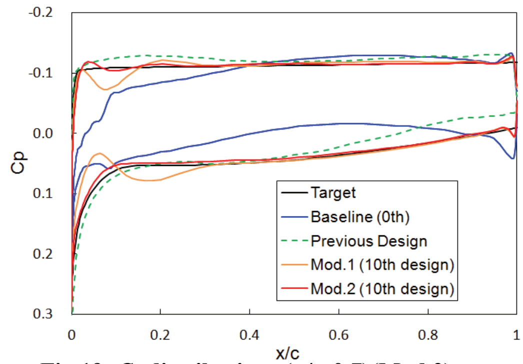

Fig 19. C_P distributions (y/s=0.7)(Mod.2)

3.3 Lift to drag ratio

Then lift to drag ratio of the designed shape (Mod.2) is investigated. Figure 20 shows the lift coefficient C_L, the pressure drag coefficient multiplied by 10 (C_{Dp} x10) and the lift to drag based on pressure drag L/D_P from the CFD analysis assumed as fully turbulent flow. In this CFD analysis, the friction drag is also calculated by the CFD analyses which have 43 drag counts in all cases. If the NLF wing design concepts are achieved in some cases, they have laminar flow region and turbulent flow region. Thus, the friction drag assumed fully turbulent flow become meaningless. So, it is the reason that the pressure drag component is only shown in Fig.20. From the 0th to 1st design, the lift and the drag are rapidly increased. As a result of the lift and drag changing, the lift to drag ratio is rapidly increased by the 1st design. The differential pressure distributions between the upper surface and lower surface on each wing section are determined by Carlson's warped wing design concepts based on the non-thickness and flat wing without the fuselage. The baseline configuration (0th) is lost the effect the warped wing, because the actual airplane has wings with thickness and camber, and also the fuselage. The reason of the increasing of the lift to drag ration at 1st design is to take into account of the effect of wing thickness and camber and fuselage in the inverse design by using the differential pressure distributions of the warped wing design. Although the lift to drag is slightly decreased after the 1st design, it still keeps higher than that of the 0th configuration and the gain of the *L/D* from the 0th design to the 10th design is 0.25. Thus, it is found the lift to drag is also improved by the inverse design method.

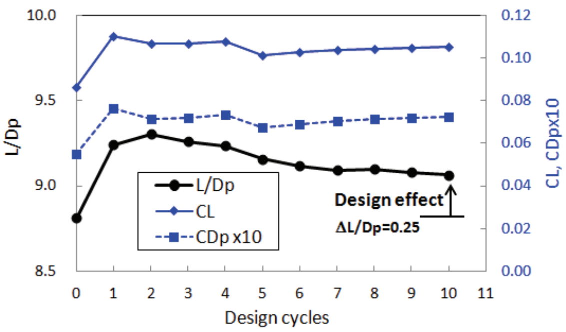

Fig 20. History of Lift to Drag ratio (Mod.2)

3.4 Transition analysis

The boundary layer transition is estimated by current e^N method based on linear stability theory. Figure 21 and 22 show the estimated boundary layer transition based on each C_P distribution and an assumption of judge condition of N=14 at the different *Re* number conditions which are corresponding to altitude, H=15km(design point) and 18km(the flight test condition) respectively. Unfortunately, some cross sections are not able to obtain its transition location because of its computational problem.

First of all, let us see the design point condition (Fig.21). In the out-board, the transition locations of the "Mod.1" are located forwarder than the "Target" ones and close to the "Baseline(0th)" ones due to the oscillation of the C_P distribution. Even the "Previous" design results around the out-board transits on the forwarder than the target ones. The C_P distribution around the out-board region of the previous design was not converged and was not able to perform further design because of the limited design term when it was conducted decades ago. This is the reason of the forward transition locations around the out-board wing. On the other hand, the "Mod.2" around the out-board wing is similar to the target due to the effect of the suppressed C_P oscillation. It is suggested that the NLF design is successfully conducted by the modification of the design method.

Next, let us see the flight test condition whose altitude is H=18km (Fig.22). In this condition, the transition locations of the design shape are similar to the target ones. In spite of the difference of the C_P distribution at y/s=0.7 of the "Mod.1", it is found that the transition locations of the previous design and present modified design results agree well with the predicted transition points based on the target C_P distribution.

Figure 23 shows ratio by the laminar flow area($S_{lam.}$) and the all upper surface area(S_{up}) on the wing at the H=18km conditions. They are only considered the upper wing surface from y/s=0.2 to y/s=0.9. It is found all of the design shapes have over 60% of laminar region. At the final analysis, these results indicate that the modified design method works well and reduces workload without any "human" optimization.

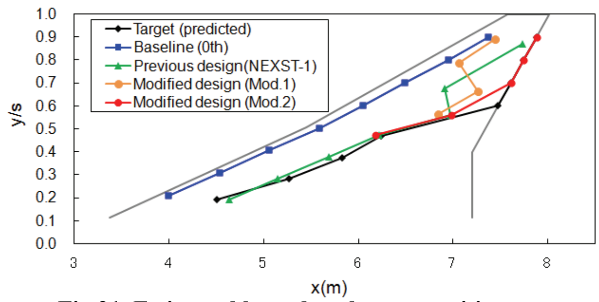

Fig 21. Estimated boundary layer transition on-set (*N*=14) (*H*=15km, Design point)

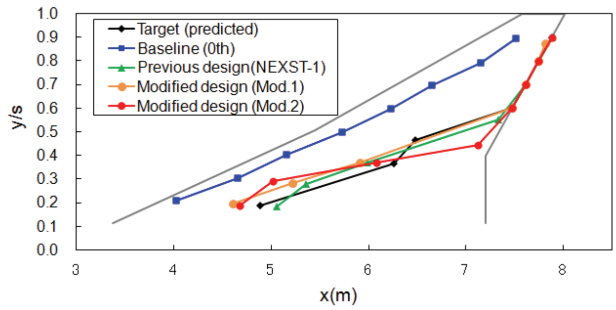

Fig 22. Estimated boundary layer transition on-set (*N*=14) (*H*=18km, Flight condition)

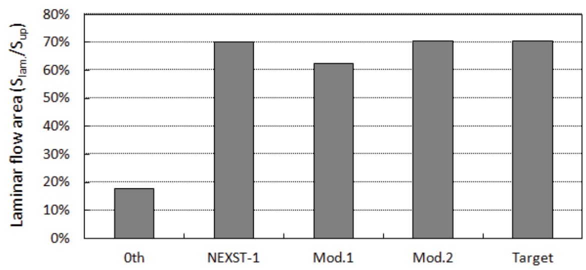

Fig 23. Laminar flow area (*N*=14) (*H*=18km)

4 Conclusion

The supersonic NLF wing design method is modified and applied to the NEXST-1 airplane. The workload and time are drastically decreased by applying the surface smoothing and grid generation systems in spite of the accuracy becomes higher than the previous method. The required time per one cycle of the NLF design becomes from 1 week to 1 day. It is found that the suitable relaxation for the geometry correction is important to obtain the converged design shape. The estimated laminar flow region by the modified design method without any "human" optimization is improved compared with the NEXST-1 airplane which is designed by previous method. Therefore, it is suggested that present efficient design system can be applied to the higher *Re* number of supersonic transport.

Acknowledgments

The authors would like to acknowledgment Dr. N. Tokugawa for her valuable advice, and Dr. Y. Ueda for his support of the analysis about the boundary layer transition.

References

[1] Ohnuki T, Hirako K and Sakata K. National Experimental Supersonic Transport Project. *Proceedings of International Congress of the Aeronautical Science*, 2006-1.4.1, Sep. 2006.

[2] Ishikawa H, Kwak D.-Y and Yoshida K. Numerical Analysis on Flight-Test Results of Supersonic Experimental Airplane NEXST-1. *AIAA Journal of Aircraft*, Vol.45, No.5, 2008, pp. 1505, 1513

[3] Kuchemann D. *The Aerodynamic Design of Aircraft*. Pergamon Press, ,June, 1978

[4] Carlson H.W and Miller D.S. Numerical Method for the Design and Analysis of Wings at Supersonic Speed. *NASA TN* D-7713, 1974

[5] Ashley H and Landahl M. *Aerodynamics of Wings and Bodies*. Dover Publications Inc., 1965

[6] Yoshida K, Iwamiya T, Ueda Y and Ishikawa H. Boundary layer transition analysis of the scaled supersonic experimental airplane. *NAL's 2nd SST-CFD Workshop*, 85-90, 2000

[7] Ueda Y, Ishikawa H and Yoshida K. Three dimensional Boundary Layer Transition Analysis in Supersonic Flow Using a Navier-Stokes Code. *Proceedings of International Congress of the Aeronautical Science*, 2004-2.8.2, Sep. 2006.

[8] Matsushima, K., Iwamiya, T. and Nakahashi, K, "Wing design for supersonic transition using integral equation method," Engineering Analysis with Boundary Elements 28(2004) 247-255, 2004

[9] Takaki R, Yamamoto K, Yamane T, Enomoto S and Mukai J. The Development of the UPACS CFD Enviroment. *High Performance Computing, Proc. Of ISHPC 2003*, Springer, pp.307-319, 2003.

[10] Baldwin B.S and Lomax H. Thin Layer Approximation and Algebraic Model for Separated Turbulent Flows. *AIAA 16th Aerospace Sciences Meeting*, Huntsville, Alabama, January 16-18, 1978.

[11] Imai I. *Conformal mappings and their applications* (in Japanese). Iwanami Shoten, Tokyo, 1979

[12] Squyers R. *Potential Flow Generation about Two-dimensional Airfoil Profiles Using the Isao Imai Conformal Transformation*. University of Texas at Arlington., 1980

Copyright Statement